24th INTERNATIONAL CONGRESS ON SOUND AND VIBRATION
23–27 July 2017, London

ICSV24
23-27JULY 2017
LONDON CALLING

NUMERICAL INVESTIGATION OF THE ACOUSTIC SCATTERING BEHAVIOR OF A BUTTERFLY VALVE

Hervé Denayer, María Muriel Gracia and Wim Desmet
KU Leuven & Member of Flanders Make, Department of Mechanical Engineering, Celestijnenlaan 300 box 2420, Leuven, Belgium
email: herve.denayer@kuleuven.be

Reinaldo Marcondes Orselli and Wim De Roeck
KU Leuven, Department of Mechanical Engineering, Celestijnenlaan 300 box 2420, Leuven, Belgium

In this paper, the scattering behavior of a butterfly valve is investigated numerically. This is done within the multi-port characterization framework, where the transmission and reflection of all cut-on modes in the inlet and outlet duct is described by a scatter matrix relation. The multi-port characteristics of the valve are computed using a set of independent simulations, carried out with an in-house Runge-Kutta discontinuous Galerkin solver for the linearized Euler equations in time-domain. In order to fully benefit from the time-domain formulation, the impulse response approach is used: a broadband pulse excitation is imposed and the simulation runs until all energy has left the system. The multi-port characteristics are computed from the time-history of the pressure, stored at a well-chosen set of positions in the inlet and outlet duct. Due to the multi-modal character of the multi-port framework, the application of the impulse response technique is less straightforward than in a plane wave propagation context. However, these issues can be overcome using appropriate signal processing techniques. In this paper, this approach is validated by comparing the simulated multi-port characteristics of a butterfly valve to an experimental reference, yielding a good agreement over the whole frequency range of interest.

Keywords: multi-port characterization, Runge Kutta discontinuous Galerkin method, time-domain simulations, linearized Euler equations

1. Introduction

In many applications, a flow duct system is the main transmission path for the noise generated upstream to the receiver. When designing such systems, two-port models in a network modeling framework are commonly adopted [1, 2]. The two-port representation of an element describes the transmission and reflection properties of a component, independent of the upstream and downstream impedance. Therefore, these models can be used in a network modeling context to reconstruct the behavior of the complete flow duct system from the representations of the individual components. However, the two-port formalism relies on the assumption of plane wave propagation in the inlet and outlet duct and is therefore only valid at low frequencies, below the first cut-off frequency. To overcome this frequency restriction, the multi-port formalism [3–5] has recently been presented as an extension of the two-port model, accounting for all cut-on modes in the inlet and outlet duct.

The multi-port characterization technique has been applied experimentally [4–7] and based on frequency-domain simulations [4]. However, although the multi-port characterization framework is defined in frequency-domain, a time-domain formulation is often preferred for broadband simulations.

Therefore, a multi-port characterization procedure using time-domain simulations has recently been presented [3]. In this paper, this time-domain characterization technique is applied to study the passive acoustic behavior of a butterfly valve from an aircraft environmental control system. Besides the detailed geometry of this industrial valve, studied within the IDEALVENT project [8], a simplified geometry is considered to investigate the influence of the small-scale geometrical details.

This paper is structured as follows. The following section first presents the multi-port framework and the characterization procedure. Section 3 details the geometry of the butterfly valve and the numerical configuration. Section 4 presents and discusses the results obtained. Finally, section 5 concludes the paper with a summary of the main conclusions.

2. Multi-port representation of a flow duct component

The multi-port formalism [3–5] is an extension to higher frequencies of the well-known two-port characterization framework [1, 2]. It considers the configuration shown in Fig. 1, where an acoustic element is mounted between two straight ducts with rigid walls.

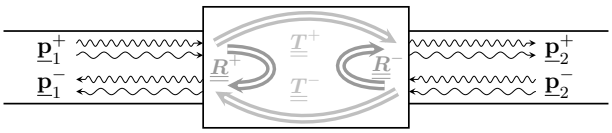

Figure 1: Multi-port element.

Within the inlet and outlet duct, the acoustic pressure field p' in frequency domain can be written as an infinite sum of duct modes:

$$p'(\omega, \vec{x}) = \sum_{m,n} p_{mn}^+(\omega)\Psi_{mn}(\omega, r, \phi)\, e^{-jk_{mn}^+ z} + p_{mn}^-(\omega)\Psi_{mn}(\omega, r, \phi)\, e^{jk_{mn}^- z} \tag{1}$$

Each duct mode describes a certain pattern in the cross section Ψ_{mn} and has an associated wavenumber $k_{mn}^{\pm}$ in the axial direction z. The subscripts $\bullet^+$ and $\bullet^-$ refer to, respectively, downstream and upstream propagation. For a duct with a circular cross section with radius R, these modes Ψ_{mn} and their propagation constants $k_{mn}^{\pm}$ are expressed as:

$$\Psi_{mn}(\omega, r, \phi) = C_{mn} J_m\left(\alpha_{mn}\frac{r}{R}\right) e^{jm\phi} \qquad k_{mn}^{\pm} = \frac{\mp M_0 k_0 + \sqrt{k_0^2 - (1 - M_0^2)\left(\frac{\alpha_{mn}}{R}\right)^2}}{1 - M_0^2}, \tag{2}$$

where $C_{mn} = \left[\left(1 - (m/\alpha_{mn})^2\right)\left(J_m(\alpha_{mn})\right)^2\right]^{-1/2}$ is a scaling factor to normalize the energy content of the modes, M_0 is the mean flow Mach number, $k_0 = \omega/c_0$ is the acoustic wavenumber, J_m is the Bessel function of the first kind of order m and α_{mn} is the $(n-1)$th zero of the first derivative of the Bessel function $J_m(x)$.

At any frequency, only a limited set of "cut-on modes" has a real axial wavenumber. The other "cut-off" modes are decaying in the axial direction and are therefore neglected within the multi-port framework. With this assumption, Eq. (1) can be written in vector formulation as:

$$p'(\omega, \vec{x}) = \underline{\boldsymbol{\Psi}}(\vec{x})\, \underline{\boldsymbol{p}}^+(\omega) + \underline{\boldsymbol{\Psi}}(\vec{x})\, \underline{\boldsymbol{p}}^-(\omega) \tag{3}$$

The modal amplitude vectors $\underline{\boldsymbol{p}}^+(\omega)$ and $\underline{\boldsymbol{p}}^-(\omega)$ contain the complex amplitudes p_{mn}^+ and p_{mn}^- of, respectively, the downstream and upstream propagating cut-on modes in the ducts. The corresponding duct modes are grouped in the vectors $\underline{\boldsymbol{\Psi}}$. The size of these vectors is determined by the number of cut-on modes N and depends on the frequency. At every cut-off frequency $f_{mn}^c = c_0\,\alpha_{mn}/(2\pi R)$, additional modes become cut-on and the size of the vectors increases.

2.1 Multi-port characterization

The multi-port representation describes the scattering behavior of a duct component using a linear matrix relation in frequency domain. The most common formulation uses the scatter matrix $\underline{\underline{\boldsymbol{S}}}$, relating the modal amplitude vectors at the inlet and outlet of the element [3–5]:

$$\begin{bmatrix} \underline{\boldsymbol{p}}_o^+(\omega) \\ \underline{\boldsymbol{p}}_i^-(\omega) \end{bmatrix} = \underline{\underline{\boldsymbol{S}}} \begin{bmatrix} \underline{\boldsymbol{p}}_i^+(\omega) \\ \underline{\boldsymbol{p}}_o^-(\omega) \end{bmatrix} \qquad \underline{\underline{\boldsymbol{S}}} = \begin{bmatrix} \underline{\underline{\boldsymbol{T}}}^+(\omega) & \underline{\underline{\boldsymbol{R}}}^-(\omega) \\ \underline{\underline{\boldsymbol{R}}}^+(\omega) & \underline{\underline{\boldsymbol{T}}}^-(\omega) \end{bmatrix} \tag{4}$$

In this equation, the subscripts $\bullet_i$ and $\bullet_o$ refer to the inlet and outlet duct. The coefficients of the scatter matrix have a direct physical interpretation. The matrices $\underline{\underline{\boldsymbol{T}}}^+$ and $\underline{\underline{\boldsymbol{T}}}^-$ describe how the incident duct modes are transmitted through the element in, respectively, the downstream and upstream direction. The matrices $\underline{\underline{\boldsymbol{R}}}^+$ and $\underline{\underline{\boldsymbol{R}}}^-$ represent the reflection of the duct modes at, respectively, the inlet and the outlet of the element.

The $(2N)^2$ coefficients of the scatter matrix can be computed from $2N$ linearly independent sets of modal amplitude vectors, representing an equal number of independent states of the system:

$$\begin{bmatrix} \underline{\underline{\boldsymbol{T}}}^+(\omega) & \underline{\underline{\boldsymbol{R}}}^-(\omega) \\ \underline{\underline{\boldsymbol{R}}}^+(\omega) & \underline{\underline{\boldsymbol{T}}}^-(\omega) \end{bmatrix} = \begin{bmatrix} \underline{\boldsymbol{p}}_{o,1}^+(\omega) & \cdots & \underline{\boldsymbol{p}}_{o,2N}^+(\omega) \\ \underline{\boldsymbol{p}}_{i,1}^-(\omega) & \cdots & \underline{\boldsymbol{p}}_{i,2N}^-(\omega) \end{bmatrix} \begin{bmatrix} \underline{\boldsymbol{p}}_{i,1}^+(\omega) & \cdots & \underline{\boldsymbol{p}}_{i,2N}^+(\omega) \\ \underline{\boldsymbol{p}}_{o,1}^-(\omega) & \cdots & \underline{\boldsymbol{p}}_{o,2N}^-(\omega) \end{bmatrix}^{-1} \tag{5}$$

In a numerical context, the independent states refer to simulations with a different excitation ("multiple source method") [4] or downstream impedance [5] ("multiple load method"). For each state of the system, the modal amplitudes are computed from the simulated pressure field. By writing Eq. (3) for $2N$ independent positions in the inlet and the outlet duct, a determined linear system of equations is obtained:

$$\begin{bmatrix} \underline{\boldsymbol{p}}^+(\omega) \\ \underline{\boldsymbol{p}}^-(\omega) \end{bmatrix} = \begin{bmatrix} \underline{\boldsymbol{\Psi}}^+(\omega, \vec{x}_1) & \underline{\boldsymbol{\Psi}}^-(\omega, \vec{x}_1) \\ \vdots & \vdots \\ \underline{\boldsymbol{\Psi}}^+(\omega, \vec{x}_{2N}) & \underline{\boldsymbol{\Psi}}^-(\omega, \vec{x}_{2N}) \end{bmatrix}^{-1} \begin{bmatrix} p'(\omega, \vec{x}_1) \\ \vdots \\ p'(\omega, \vec{x}_{2N}) \end{bmatrix} \tag{6}$$

The positions $\vec{x}_i$ have to be chosen to ensure the modal matrix is invertible for all frequencies of interest. This task can be facilitated by using more than $2N$ positions and solving the overdetermined matrix equation using a Moore-Penrose pseudoinverse. However, the modal matrix is unavoidably singular at the cut-off frequencies [4] and the multi-port characterization technique can therefore not be applied at these discrete frequencies.

2.2 Multi-port characterization using time-domain simulations

Although the multi-port framework is defined in frequency domain, a time-domain formulation offers advantages for broadband simulations. Therefore, the multi-port characterization of the butterfly valve is carried out using the impulse response method [3]. Each state in Eq. (5) refers to a simulation excited by a pulse at a predefined point in the inlet or outlet duct. The simulation runs until most of the acoustic energy has left the numerical domain through the non-reflecting inlet and outlet, or by numerical dissipation. The time history of the pressure is stored at a set of points in the inlet and outlet duct and the modal decomposition is carried out using the FFT transform of the converged pressure signals at these points in Eq. (6).

However, the multi-modal nature of the pressure field poses an issue for the impulse response technique [3]. The group velocity of a duct mode equals zero at the cut-off frequency. As a result, the energy injected in a mode at this frequency will not propagate axially and can only leave the domain by numerical dissipation. Fortunately, these frequencies are of no interest for the multi-port characterization because of the singular modal matrix. The time series can therefore be treated as converged as soon as most of the energy contained in the other frequencies has left the domain. A Hanning window is then applied to these partially converged signal to suppress leakage.

3. Numerical configuration

In this paper, the numerical multi-port characterization is applied to a butterfly valve of an aircraft environmental control system. This valve, studied in detail within the IDEALVENT project [8], has an inner diameter of $D = 85$ mm. The opening angle of the valve has been fixed to 30°, where 0° refers to the fully closed position. Besides the detailed geometry of this industrial valve, shown in Fig. 2(a), also a simplified geometry has been considered. As shown in Fig. 2(b), all small-scale geometrical features and the curvature of the surface are neglected and the valve is represented by a flat circular plate.

(a) (b)

Figure 2: Surface discretization around the butterfly valve for (a) the detailed geometry and (b) the simplified geometry.

The simulations are carried out with a Runge-Kutta discontinuous Galerkin discretization of the linearized Euler equations (LEE) in time-domain [9, 10]. The equations are solved on an unstructured tetrahedral grid using 4th order polynomial shape functions. Within the spatial DG discretization, linear elements are used throughout the numerical domain and second-order elements [11] are used locally to represent the curved wall of the duct without the need for excessive mesh refinement. Close to the valve, second-order elements are not needed for an accurate representation of the geometry because of the small element size. This mixed approach offers an optimal compromise between the computational efficiency of the quadrature-free formulation for the linear elements and the geometrical accuracy of the second-order elements [12]. Lax-Friedrich fluxes are used for the inter-element communication and an 8 step 4th order Runge-Kutta scheme, optimized for the spatial DG operator [13], is used for the time integration.

The computational domain consists of a duct with a diameter of $D = 85$ mm and a length of $40D$, complemented with a damping zone of length $9D$ at the inlet and outlet to suppress reflections. The valve is positioned in the center of this domain. An unstructured mesh with 71731 and 44171 tetrahedral elements is generated and partitioned using gmsh [14] for, respectively, the detailed and the simplified valve geometry. All walls are represented by slip boundary conditions and the inlet and outlet are modeled using characteristic non-reflecting boundary conditions.

The valve is characterized up to the second cut-off frequency of the inlet and outlet duct (approximately 3950 Hz). As such, up to three modes can be cut-on: the plane mode (0,0), the first azimuthal mode (1,0) and its complex conjugate (-1,0). Therefore, at least six independent simulations are required to compute all scatter matrix coefficients. This is achieved using a multiple source approach, by varying the position of the excitation. Each simulation is excited by a pulse in the inlet or outlet duct, located at a distance of $12.5D$ of the center of the valve and at $0.3D$ of the center-line of the duct. Three simulations use an upstream pulse, at respectively 30°, 150° and 270° with respect to the rotation axis of the valve. The remaining three simulations use a downstream excitation at, respectively, 30°, 150° and 270°.

The time history of the pressure is stored at 30 points in the inlet and in the outlet duct. These points are distributed evenly over 5 cross-sections at $5.05D$, $5.5D$, $6D$, $7.7D$ and $8.1D$ from the center of the valve. Within each of these cross-sections, 6 points are located every 60° at $0.375D$

from the center-line of the duct. After windowing, an FFT algorithm is applied to the time history of the pressure at these points and the modal decomposition is carried out by using the obtained pressure spectra in the overdetermined Eq. (6).

At the current stage, only quiescent conditions have been considered. In ongoing research, the multi-port characteristics of the butterfly valve are being computed for a mean flow with a Mach number of $M = 0.1$. The mean flow field, obtained from a RANS simulation [15], is mapped from the fine CFD grid to the coarser mesh for the acoustic simulations using the three-dimensional least-squares procedure, recently presented in reference [16]. To suppress instabilities caused by the strongly non-uniform flow around the valve, the envisaged simulations use a Runge-Kutta discontinuous Galerkin solver for the linearized Navier-Stokes equations [10], instead of the LEE.

4. Results and discussion

Figure 3 shows the diagonal elements of the transmission matrices $\underline{\underline{\boldsymbol{T}}}^{+}$ and $\underline{\underline{\boldsymbol{T}}}^{-}$, representing the transmission coefficients of the plane mode, the first azimuthal mode and its complex conjugate to their counterparts at the other side of the butterfly valve. Figure 4 shows the corresponding reflection coefficients. For all coefficients, the simplified geometry presents a reasonable approximation and predicts the correct trends, but it is clear that the results of the detailed geometry are in better agreement with the experimental reference solution [6, 8].

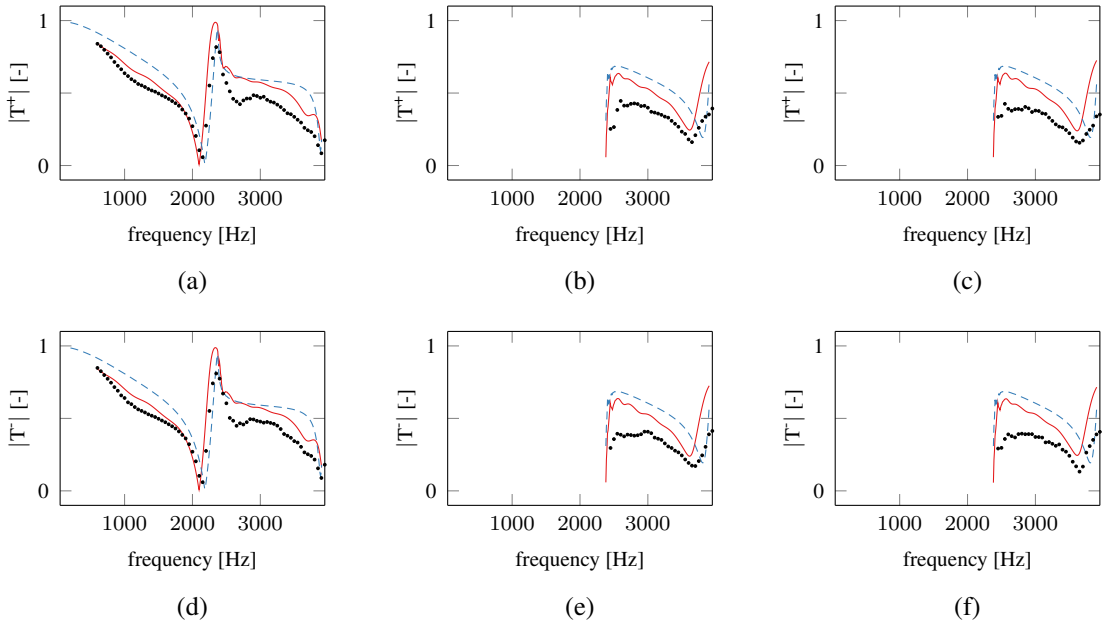

Figure 3: Measured transmission coefficients of the butterfly valve (·) and simulated transmission coefficients for the detailed geometry (——) and the simplified geometry (- - - -) for the downstream propagating (a) (0,0) mode, (b) (1,0)-mode and (c) (-1,0)-mode and the upstream propagating (d) (0,0) mode, (e) (1,0)-mode and (f) (-1,0)-mode.

At low frequencies, the valve is acoustically compact and behaves as an area restriction in a duct: the transmission coefficient gradually decreases with frequency, with a corresponding increase of the reflection coefficients [17]. At higher frequencies, the acoustic wavelength is of the same order of magnitude as the length of the valve and interference between the acoustic waves propagating on both sides of the valve can occur. Around 2100 Hz, still within the plane wave region, the transmission coefficients of the plane mode suddenly drop to nearly zero. This phenomenon is caused by the existence of embedded modes [7, 18], which can be excited by an incident plane wave for a partially opened butterfly valve.

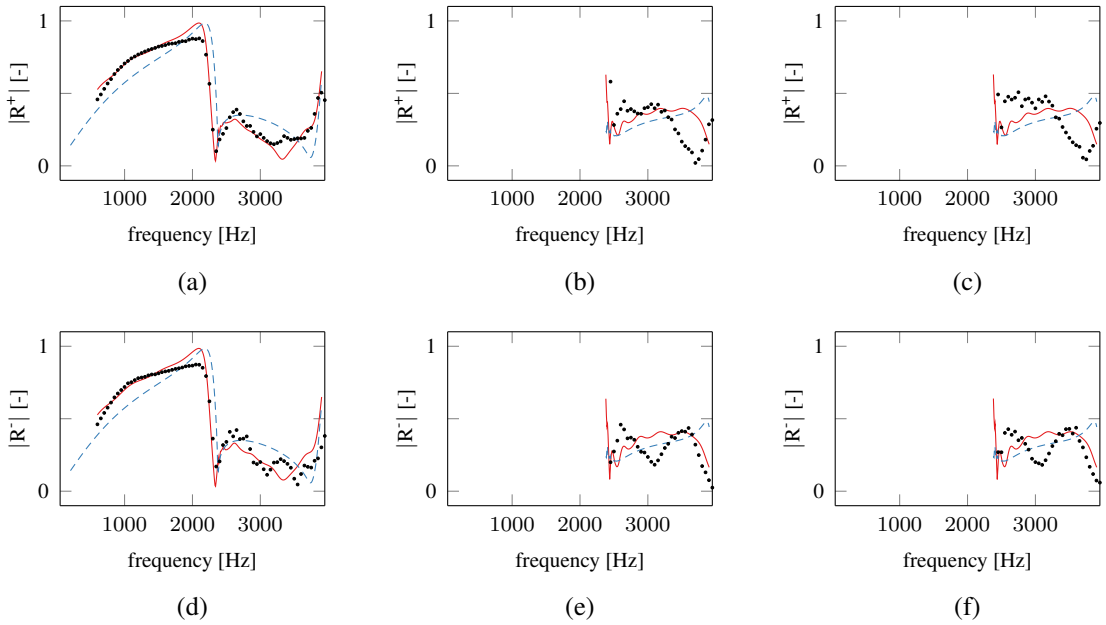

Figure 4: Measured reflection coefficients of the butterfly valve (·) and simulated reflection coefficients for the detailed geometry (——) and the simplified geometry (- - - -) for the downstream propagating (a) (0,0) mode, (b) (1,0)-mode and (c) (-1,0)-mode and the upstream propagating (d) (0,0) mode, (e) (1,0)-mode and (f) (-1,0)-mode.

Above the cut-off frequency, also the first azimuthal mode (1,0) and its complex conjugate (-1,0) are cut-on. In this frequency region, the discrepancies between the simulations and the experimental reference are more pronounced. This is mainly due to the increased importance of visco-thermal wall losses, which are neglected in the numerical model. The simulations correctly predict a symmetrical and reciprocal behavior of the transmission coefficients. However, the clear difference between the upstream and downstream reflection coefficients is not captured by the simulations.

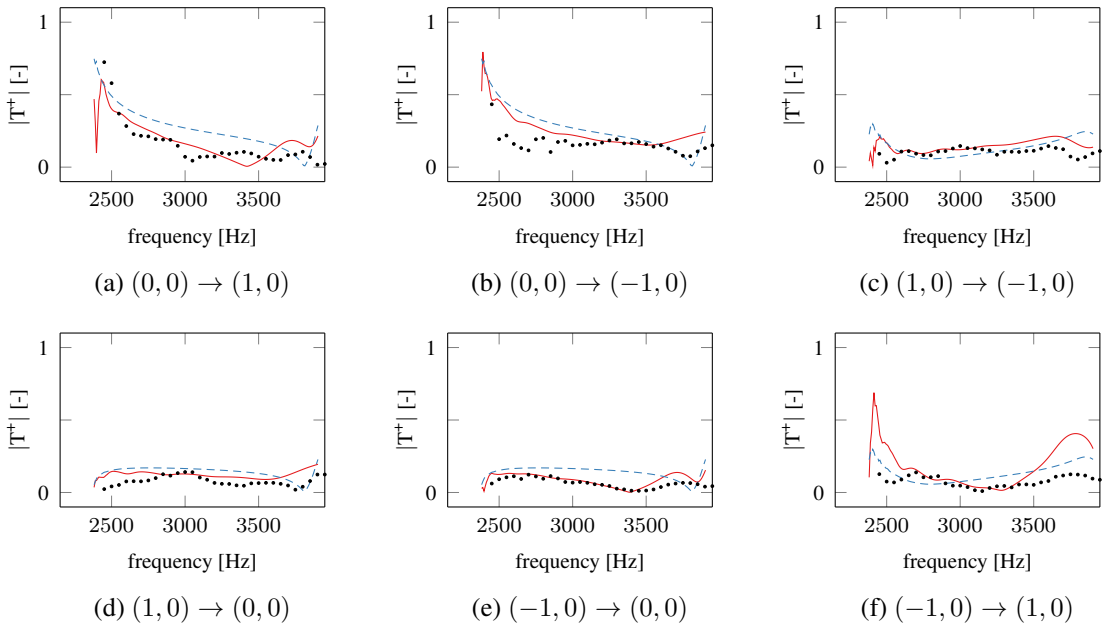

Figure 5: Measured conversion coefficients in the transmission matrix $\underline{\underline{\boldsymbol{T}}}^{+}$ of the butterfly valve (·) and simulated conversion coefficients for the detailed geometry (——) and the simplified geometry (- - - -) for the downstream propagating modes.

Figures 3 and 4 only considered the diagonal terms of the transmission and reflection matrices, representing the transmission and reflection of a duct mode to itself. The other terms of these matrices, shown in Figs. 5 and 6, represent the conversion of a duct mode to the other duct modes. Since only the plane mode is cut-on at low frequencies, these conversion coefficients only exist beyond the cut-off frequency.

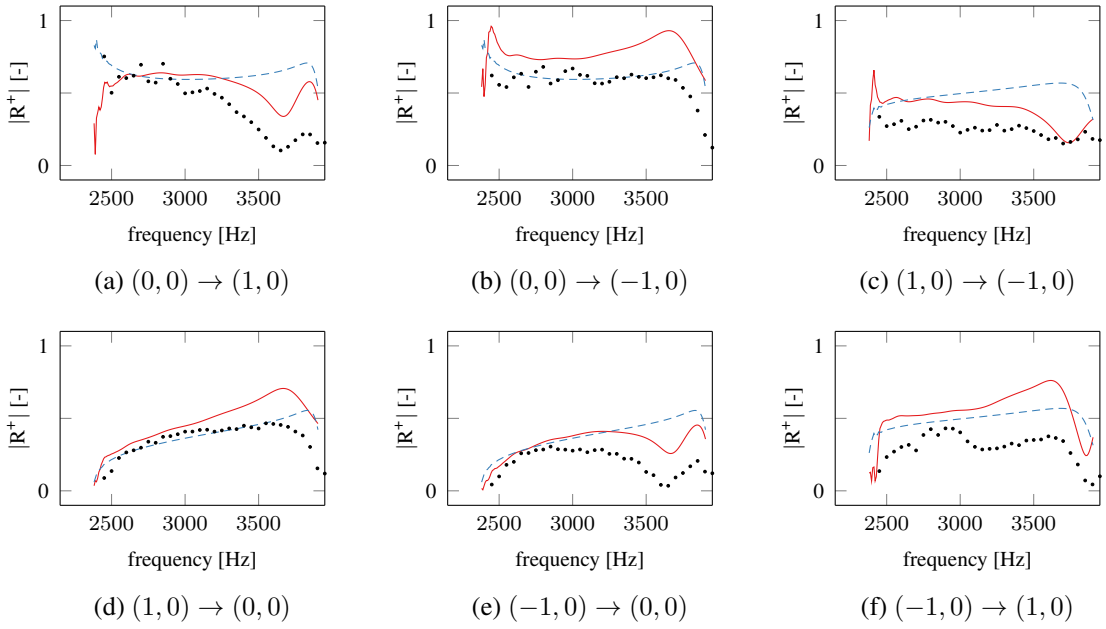

(a) $(0,0) \rightarrow (1,0)$ (b) $(0,0) \rightarrow (-1,0)$ (c) $(1,0) \rightarrow (-1,0)$

(d) $(1,0) \rightarrow (0,0)$ (e) $(-1,0) \rightarrow (0,0)$ (f) $(-1,0) \rightarrow (1,0)$

Figure 6: Measured conversion coefficients in the reflection matrix $\underline{\underline{\boldsymbol{R}}}^{+}$ of the butterfly valve (·) and simulated conversion coefficients for the detailed geometry (——) and the simplified geometry (- - - -) for the downstream propagating modes.

As shown in Fig. 5, only a minor conversion between the different modes occurs in the transmission matrix. For the simplified geometry, the conversion coefficients follow the expected symmetry: the conversion between the plane mode and the two azimuthal modes is identical and the same holds for the conversion coefficients between the two azimuthal modes. For the detailed geometry, significant asymmetries can be observed, especially at higher frequencies. This is caused by the geometrical details, which are different on both sides of the valve and no longer acoustically compact at high frequencies. This asymmetry is also observed experimentally.

More pronounced conversion between the modes can be observed in the reflection matrix, as shown in Fig. 6. Also here, the results of the simplified valve geometry are identical for both azimuthal modes. The detailed geometry however correctly captures the clear differences between these modes, observed in the experiments.

5. Conclusions

In this paper, a novel multi-port characterization technique, based on time-domain simulations, is applied to study the passive acoustic behavior of a butterfly valve. The simulations are carried out with a Runge-Kutta discontinuous Galerkin discretization of the linearized Euler equations in time-domain, using a pulse to generate a broadband excitation. The computed transmission, reflection and conversion coefficients of the different cut-on modes are in good agreement with the experimental reference for the whole frequency range of interest. Besides the detailed geometry, a simplified model has been considered where the valve is represented by a flat circular plate. As expected, this model yields only a qualitative agreement with the reference solution and illustrates the importance of the geometrical details, especially at higher frequencies. As such, these examples show that the multi-port

characterization approach using time-domain simulations is ideally suited for an efficient, broadband characterization of complex flow duct components.

ACKNOWLEDGEMENTS

The authors acknowledge the support of the EU Seventh Framework Programme under the Level 1 Collaborative Project IDEALVENT (GA 314066). The Research Fund KU Leuven and the Flanders Innovation & Entrepreneurship Agency, within the TUMULT project, are gratefully acknowledged for their support. The research of R.M. Orselli is funded by a Fellowship of the Brazilian Science without Borders program (CNPq 2491272013-0). This research was partially supported by Flanders Make, the strategic research centre for the manufacturing industry

REFERENCES

1. Munjal, M., *Acoustics of Ducts and Mufflers with Application to Exhaust and Ventilation System Design*, John Wiley & Sons (1987).
2. Åbom, M. Measurement of the scattering-matrix of acoustical two-ports, *Mechanical Systems and Signal Processing*, **5** (2), 89–104, (1991).
3. Denayer, H., Korchagin, V., Orselli, R., De Roeck, W. and Desmet, W. Acoustic multi-port characterization of flow duct systems based on time-domain simulations, *Journal of Sound and Vibration*, **submitted**, (2017).
4. Sack, S. and Åbom, M. On acoustic multi-port characterisation including higher order modes, *Acta Acustica united with Acustica*, **102** (5), 834–850, (2016).
5. Sitel, A., Ville, J.-M. and Foucart, F. Multiload procedure to measure the acoustic scattering matrix of a duct discontinuity for higher order mode propagation conditions, *Journal of the Acoustical Society of America*, **120** (5), 2478–2490, (2006).
6. Denayer, H., De Roeck, W. and Desmet, W. Active multi-port characterization of a butterfly valve, *Proceedings of the International Conference on Noise and Vibration Engineering ISMA 2016*, pp. 317–330, (2016).
7. Bennouna, S., *Caractérisation aéroacoustique d'éléments et associations d'éléments de systèmes de ventilation d'air pour l'automobile*, Ph.D. thesis, (2016).
8. IDEALVENT, (2014), *WP2 final report (public) - Experimental characterization of flow-acoustic and multi-component interactions*.
9. Reymen, Y., *3D High-order Discontinuous Galerkin Methods for Time-Domain Simulation of Flow Noise Propagation*, Ph.D. thesis, K.U. Leuven, (2008).
10. Toulorge, T., *Efficient Runge-Kutta Discontinuous Galerkin Methods Applied to Aeroacoustics*, Ph.D. thesis, KU Leuven, (2012).
11. Toulorge, T. and Desmet, W. Curved boundary treatments for the discontinuous Galerkin method applied to aeroacoustic propagation, *AIAA Journal*, **48**, 479–489, (2010).
12. De Roeck, W., Denayer, H., Pluymers, B. and Desmet, W. Analysis of the aeroacoustic behavior of flow duct systems using an active multi-port characterization, *Proceedings of the Aachen Acoustics Colloquium 2015*, (2015).
13. Toulorge, T. and Desmet, W. Optimal Runge-Kutta schemes for discontinuous Galerkin space discretizations applied to wave propagation problems, *Journal of Computational Physics*, **231** (4), 2067–2091, (2012).
14. Geuzaine, C. and Remacle, J.-F. Gmsh: a three-dimensional finite element mesh generator with built-in pre- and post-processing facilities, *International Journal for Numerical Methods in Engineering*, **79**, 1309–1331, (2009).
15. IDEALVENT, (2014), *WP4 final report (public) - Simulation of the flow and acoustic interactions in the combined configuration*.
16. Muriel Gracia, M., Denayer, H., De Roeck, W. and Desmet, W. Validation of an accurate mapping scheme to couple CFD data to DG solvers for aeroacoustic propagation, *23rd AIAA/CEAS Aeroacoustics Conference*, (2017).
17. Ajello, G., *Mesures acoustiques dans les guides d'ondes en présence d'écoulement: Mise au point d'un banc de mesure: Applications à des discontinuités*, Ph.D. thesis, Université du Maine, (1997).
18. Duan, Y., Koch, W., Linton, C. M. and McIver, M. Complex resonances and trapped modes in ducted domains, *Journal of Fluid Mechanics*, **571**, 119–147, (2007).